Available online at www.sciencedirect.com

Journal of Applied Research and Technology

Journal of Applied Research and Technology 15 (2017) 464–476

www.jart.ccadet.unam.mx

Original

Double stratification effects on unsteady electrical MHD mixed convection flow of nanofluid with viscous dissipation and Joule heating

Yahaya Shagaiya Daniel [a,b], Zainal Abdul Aziz [a,b,*], Zuhaila Ismail [a,b], Faisal Salah [c]

[a] *Department of Mathematical Science, Faculty of Sciences, Universiti Teknologi Malaysia, UTM, 81310 Johor Bahru, Johor, Malaysia*
[b] *UTM Centre for Industrial and Applied Mathematics, Universiti Teknologi Malaysia, UTM, 81310 Johor Bahru, Johor, Malaysia*
[c] *Department of Mathematics, Faculty of Science, University of Kordofan, Elobied 51111, Sudan*

Received 9 December 2016; accepted 18 May 2017
Available online 14 October 2017

Abstract

The problem of unsteady mixed convection electrical magnetohydrodynamic (MHD) flow and heat transfer induced due to nanofluid over a permeable stretching sheet using Buongiorno model is investigated. The transverse electric and magnetic fields are considered in the flow field, while in the heat convection is associated with the thermal radiation, heat generation/absorption, viscous and Ohmic dissipations, and chemical reaction is incorporated in the mass diffusion. A similarity transformation is used to reduce the boundary layer governing equations which are partial differential equations to nonlinear differential equations and then solved numerically using implicit finite difference scheme. The nanofluid velocity and temperature are sensitive to an increase in the electric field, which resolved the problem of sticky effects due to the magnetic field. Destructive chemical reaction increases the level nanoparticles concentration while reversed behave happened in the case of the generative chemical reaction. Heat source boosts the fluid temperature while as opposite occurred with the heat sink. Thermal and concentration stratifications decreased the fluid temperature and the nanoparticles concentration profiles. Buoyancy ratio parameter reduced the Nusselt and Sherwood numbers whereas mixed convection parameter increases for higher values. A comparison with the previous study available in literature has been done and found an excellent agreement with the published data.

Keywords: Magnetic nanofluid; Doubly stratified flow; Mixed convection; Thermal radiation; Electric field; Viscous and Ohmic dissipations

1. Introduction

Magnetohydrodynamic (MHD) nanofluid is an essential aspect of convective heat transfer and has numerous applications in science and engineering processes (Lin, Zheng, Zhang, Ma, & Chen, 2015). Nanofluids is a composition of nanoparticles suspended in a conventional liquid that has higher thermal conductivity in contrast with the conventional liquid (Choi, 1995). Such conventional liquid is water, oil and ethylene glycol in nature are poor in thermal conductivity, which limits the heat transfer performance. Due to innovation in technology via miniaturization of an electronic device requires the further advance of heat transfer from energy saving. To overcome this challenges leads to a new class of fluid called nanofluid. The application of magnetic field for electrical conducting nanofluid is of recent interest among different researchers (Abolbashari, Freidoonimehr, Nazari, & Rashidi, 2014; Daniel, Aziz, Ismail, & Salah, 2017a; Daniel, 2015a, 2015b, 2016, 2017; Hedayatnasab, Abnisa, & Daud, 2017; Malvandi, Hedayati, & Ganji, 2014; Sandeep & Sulochana, 2015; Waqas et al., 2016). Essential roles in sink-float separation, sealing of materials and construction of loudspeakers. The rate of heat transfer with application to the nuclear reactions and metallurgical processes is as result of its greater thermal conductivity (Shateyi & Motsa, 2011). Due to the fascinating properties possess by magnetic nanofluid of liquid and magnetic behavior (Bég, Khan, Karim, Alam, & Ferdows, 2014). Such materials have relevance applications via magneto-optical wavelength fibers, optical switches, optical modulators, nonlinear optical materials,

* Corresponding author.
E-mail address: zainalaz@utm.my (Z.A. Aziz).
Peer Review under the responsibility of Universidad Nacional Autónoma de México.

http://dx.doi.org/10.1016/j.jart.2017.05.007

Nomenclature

a,b	constants
B_0	magnetic field
$\bar{B}$	applied magnetic field
c	stretching sheet constant
c_f	skin friction coefficient
D_B	Brownian diffusion coefficient
D_T	thermophoresis diffusion coefficient
E_0	electric field factor
E_1	electric field parameter
$\bar{E}$	applied electric field
Ec	Eckert number
f'	dimensionless velocity
g	magnitude of the gravity
Gr	Grashof number
$\bar{J}$	Joule current
k	thermal conductivity
k_f, k_p	thermal conductivity of the base fluid and nanoparticle
Le	Lewis number
M	magnetic field parameter
Nb	Brownian motion parameter
Nr	buoyancy ratio parameter
Nt	thermophoresis parameter
Nu	local Nusselt number
Pr	Prandtl number
q_m	wall mass flux
q_r	radiative heat flux
q_w	wall heat flux
Rd	radiation parameter
Re_x	local Reynolds number
s	suction/injection
s_c	solutal stratification
s_t	thermal stratification
Sh	local Sherwood number
T	temperature of the fluid
T_W	constant temperature at the wall
T_∞	ambient temperature
T_0	Reference temperature
u, v	velocity component along x- and y-direction component
$\bar{V}$	velocity fluid
V_W	wall mass transfer

Greek symbols

α	thermal diffusivity
σ^*	Stefan–Boltzmann constant
σ	electrical conductivity
β	volume expansion coefficient
β_{nf}	volumetric volume expansion coefficient of the nanofluid
ε	heat generation/absorption parameter
η	dimensionless similarity variable
μ	dynamic viscosity of the fluid
υ	kinematic viscosity of the fluid
ρ, ρ_{nf}	density
ρ_p	particle density
$(\rho)_f$	density of the fluid
$(\rho c)_f$	heat capacity of the fluid
$(\rho c)_p$	effective heat capacity of a nanoparticle
ψ	stream function
σ	electrical conductivity
φ	concentration of the fluid
φ_W	nanoparticle volume fraction at the surface
φ_∞	ambient nanoparticle
φ_0	reference concentration
θ	dimensionless temperature
ϕ	dimensionless concentration
τ	ratio between the effective heat transfer capacity of the nanoparticle and the heat capacity of the fluid
τ_W	surface shear stress
λ	mixed convection parameter
γ	chemical reaction parameter

Subscripts

∞	condition at the free stream
W	condition at the wall/surface

and optical gratings. The heat conduction has an unlimited significance in numerous industrial heating or cooling equipment. Recently, the impact of magnetic field on nanofluids has also been reported by other researchers (Daniel & Daniel, 2015; Daniel, Aziz, Ismail, & Salah, 2017b; Freidoonimehr, Rashidi, & Mahmud, 2015; Gómez-Pastora et al., 2017; Hayat & Qasim, 2011; Hayat, Waqas, Khan, & Alsaedi, 2017b; Kumar & Sood, 2017; Mabood, Khan, & Ismail, 2015; Mohammed, Gomaa, Ragab, & Zhu, 2017; Shagaiy, Aziz, Ismail, & Salah, 2017).

Stratification is a deposition (formation) of layers which occur as result of different fluids mixtures, temperature variation, densities difference or concentration differences which occur in fluids (Rehman, Malik, Salahuddin, & Naseer, 2016). Physically, heat and mass transfer analysis run concurrently, it is of great interest to explore the mechanism of double stratification (thermal and mass stratifications) on the convective transport in nanofluid (Hayat, Waqas, Khan, & Alsaedi, 2016d). These draw the attention of researchers such as (Hayat, Mumtaz, Shafiq, & Alsaedi, 2017a; Mehmood, Hussain, & Sagheer, 2016; Ramzan, Bilal, & Chung, 2017) due to its frequent occurrence in various industrial and engineering processes namely heat rejection into the surrounding (environment) via rivers, lakes and seas, also thermal energy storage systems via solar ponds, condenser of power plants, industrial composition, manufacturing processing and heterogeneous composition in food,

atmospheric density stratification, etc. The random movement of nanosized particles within the conventional fluids is known as Brownian motion, which occurred as result of continuous collisions between the nanosized particles and the fluid molecules. Diffusion of particles sized under the influence of temperature gradient is called thermophoresis. Thermophoresis is a remarkable significance of the Brownian motion of nanosized particles in liquids with an externally sustained and constant temperature gradient. Buongiorno (2006) developed a two-phase nanofluid model for investigating thermal energy transport, which has been successfully used to address various diverse flow problems (Hayat, Muhammad, Shehzad, & Alsaedi, 2016b; Mabood & Khan, 2016) involving nanofluids the aspects of Brownian motion and thermophoretic diffusion. The influence of radiative heat transfer which is essential in industries at higher temperature processes subjected to isothermal and non-isothermal surroundings (Pal & Mandal, 2016). The radiative heat transfer via nanofluid play a key role in system devices and renewable energy sources (Hayat, Qayyum, Waqas, & Alsaedi, 2016c). In view of these technological and engineering widely applications drawn the attentions of some researchers (Bhatti, Zeeshan, Ijaz, Bég, & Kadir, 2016; Daniel, Aziz, Ismail, & Salah, 2017c; Hayat, Gull, Farooq, & Ahmad, 2015; Hayat, Waqas, Shehzad, & Alsaedi, 2016e; Hussain, 2017; Jing, Pan, & Wang, 2017; Khan, Tamoor, Hayat, & Alsaedi, 2017) to explore in this direction.

The aim of the current study is to investigate the combined effects of an electric field, magnetic field, thermal radiation, heat generation/absorption, chemical reaction, viscous dissipation, and Joule heating for unsteady mixed convection flow of electrical conducting nanofluid in the presence of thermal stratification and concentration stratifications over a permeable stretching sheet. Buongiorno nanofluid model is adopted which features the novel aspects of the Brownian motion and thermophoresis. Additional, water based nanofluid (Mabood et al., 2015) is used. The boundary layer governing equations which are partial differential equations are transformed into a set of nonlinear self-similar ordinary differential equations. Computational analysis is performed through implicit finite difference scheme known as Keller box method (Cebeci & Bradshaw, 2012). The effects of physical sundry parameters on the velocity, temperature, nanoparticle concentration profiles, skin friction, and Nusselt and Sherwood numbers are presented and discussed extensively with the aids of graphs and tables.

2. Mathematical formulation

Consider the unsteady mixed convection flow of an electrical conducting nanofluid over a permeable stretching sheet surface in the presence of external magnetic and electric fields, thermal radiation, heat generation/absorption, chemical reaction, viscous dissipation and Joule heating. The coordinate system is selected in such a manner that the x-axis is measured along the stretching sheet and the y-axis is normal to it and the flow is occupied above the surface sheet $y>0$ displayed in Figure 1. Two equal and opposite forces

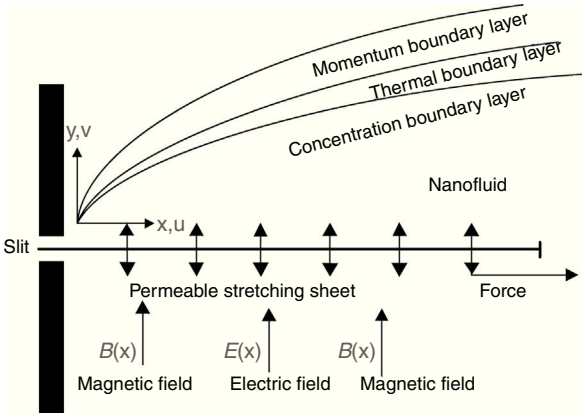

Fig. 1. Physical configuration of the geometry.

are impulsively applied along the x-axis so that the sheet is stretched with the velocity $u_W(x, t)$ along the x-axis. As the fluid is electrical conducting so the Lorentz force $\vec{J}\times\vec{B}$ where $\vec{J}=\sigma(\vec{E}+\vec{V}\times\vec{B})$ is the Joule current (electrical conducting density), σ is the electrical conductivity and $\vec{V}=(u, v)$ is the fluid velocity, $\vec{B}=(0,\quad B,\quad 0)$, $\vec{E}=(0,\quad 0,\quad -E)$ is the transverse magnetic and electric fields. The induced magnetic field and Hall current effects are ignored under small magnetic Reynolds number. Both the electric and magnetic fields due to viscous dissipation and Joule heating contributed to the momentum and thermal boundary layer equations. The sheet is main at temperature $T_W=T_0+A_1x(1-at)^{-1}$ and concentration $\varphi_W=\varphi_0+C_1x(1-at)^{-1}$. The temperature and mass concentration of the ambient fluid are assumed to be stratified in the form $T_\infty=T_0+A_2x(1-at)^{-1}$ and $\varphi_\infty=\varphi_0+C_2x(1-at)^{-1}$ respectively. In addition, the effects of thermal radiation and viscous dissipation are considered in the thermal boundary layer equation whereas chemical reaction in the concentration boundary layer equation. Using Buongiorno model, the conservative equations in the aforementioned conditions is given as:

Continuity equation

$$\frac{\partial u}{\partial x}+\frac{\partial v}{\partial y}=0 \tag{1}$$

x-Momentum equation

$$\frac{\partial u}{\partial t}+u\frac{\partial u}{\partial x}+v\frac{\partial u}{\partial y}=-\frac{1}{\rho_f}\frac{\partial P}{\partial x}+\nu\left(\frac{\partial^2 u}{\partial x^2}+\frac{\partial^2 u}{\partial y^2}\right)+\frac{\sigma}{\rho_f}\left(EB-B^2u\right)+\frac{1}{\rho_f}\left[(1-\varphi_\infty)\rho_{f\infty}\beta(T-T_\infty)-\left(\rho_p-\rho_{f\infty}\right)\beta(\varphi-\varphi_\infty)\right]g \tag{2}$$

y-Momentum equation

$$\frac{\partial v}{\partial t}+u\frac{\partial v}{\partial x}+v\frac{\partial v}{\partial y}=-\frac{1}{\rho_f}\frac{\partial P}{\partial y}+\nu\left(\frac{\partial^2 v}{\partial x^2}+\frac{\partial^2 v}{\partial y^2}\right)+\frac{\sigma}{\rho_f}\left(EB-B^2v\right)+\frac{1}{\rho_f}\left[\left(1-\varphi_\infty\right)\rho_{f\infty}\beta\left(T-T_\infty\right)-\left(\rho_p-\rho_{f\infty}\right)\beta\left(\varphi-\varphi_\infty\right)\right]g \tag{3}$$

Energy equation

$$\frac{\partial T}{\partial t}+u\frac{\partial T}{\partial x}+v\frac{\partial T}{\partial y}=\frac{k}{(\rho c)_f}\left(\frac{\partial^2 T}{\partial x^2}+\frac{\partial^2 T}{\partial y^2}\right)-\frac{1}{(\rho c)_f}\left(\frac{\partial q_r}{\partial y}\right)+\frac{\mu}{(\rho c)_f}\left(\frac{\partial u}{\partial y}\right)^2+\frac{Q}{(\rho c)_f}\left(T-T_\infty\right)+\frac{\sigma}{(\rho c)_f}(uB-E)^2+\tau\left\{D_B\left(\frac{\partial\varphi}{\partial x}\frac{\partial T}{\partial x}+\frac{\partial\varphi}{\partial y}\frac{\partial T}{\partial y}\right)+\frac{D_T}{T_\infty}\left[\left(\frac{\partial T}{\partial x}\right)^2+\left(\frac{\partial T}{\partial y}\right)^2\right]\right\} \tag{4}$$

Concentration equation

$$\frac{\partial\varphi}{\partial t}+u\frac{\partial\varphi}{\partial y}+v\frac{\partial\varphi}{\partial y}=D_B\left(\frac{\partial^2\varphi}{\partial x^2}+\frac{\partial^2\varphi}{\partial y^2}\right)+\frac{D_T}{T_\infty}\left(\frac{\partial^2 T}{\partial x^2}+\frac{\partial^2 T}{\partial y^2}\right)-k_1\left(\varphi-\varphi_\infty\right) \tag{5}$$

The boundary conditions at the sheet for the physical model are presented by

$$\begin{aligned}&y=0:\quad u=u_w(x,t),\quad v=v_w(x,t),\\&\quad T=T_W(x,t)=T_0+A_1x(1-at)^{-1},\\&\varphi=\varphi_W(x,t)=\varphi_0+C_1x(1-at)^{-1},\\&y\to\infty:\quad u\to 0,\quad T\to T_\infty=T_0+A_2x(1-at)^{-1},\\&\quad\varphi\to\varphi_\infty=\varphi_0+C_2x(1-at)^{-1}\end{aligned} \tag{6}$$

Here $u_W(x,\ t)=bx/(1-at)$ denotes the velocity of the linear stretching sheet, where b is the stretching rate, a is the positive constant with the property $(at<1)$ and dimension of a,b is T^{-1}. A_1, A_2, C_1, and C_2 are the dimensional constants with dimension L^{-1} $v_w=-v_0/\sqrt{1-at}$ is the wall mass transfer, when $v_w<0$ denote the injection while $v_w>0$ indicates the suction, $E=E_0/\sqrt{1-at}$ is the electric field and E_0 is the intensity of the electric field, and $B=B_0/\sqrt{1-at}$ is the magnetic field and B_0 is the intensity of the magnetic field. Where u and v represent the velocity components along the x-and y-axis respectively. g, P, $\alpha=k/(\rho c)_f$, μ, $\rho\,\rho_f$ and ρ_p is the gravitational acceleration, the fluid pressure, the thermal diffusivity, the kinematic viscosity, the density, the fluid density and particles density respectively. We also have D_B, D_T, $\tau=(\rho c)_p/(\rho c)_f$ which represents the Brownian diffusion coefficient, the thermophoresis diffusion coefficient, the ratio between the effective heat transfer capacity of the ultrafine nanoparticle material and is the heat capacity of the fluid and $k_1=k_0/(1-at)$, $Q=Q_0/(1-at)$ is the rate of chemical reaction and heat generation/absorption as (Q_0 is the heat generation or absorption coefficient and k_0 is the chemical reaction coefficient) respectively.

The radiative heat flux q_r via Rosseland approximation (Daniel & Daniel, 2015; Sparrow & Cess, 1978) is applied to Eq. (4), such that.

$$q_r=-\frac{4\sigma^*}{3k^*}\frac{\partial T^4}{\partial y} \tag{7}$$

where σ^* represent the Stefan–Boltzmann constant and k^* denote the mean absorption coefficient. Expanding T^4 by using Taylor's series about T_∞ and neglecting higher order terms, we have,

$$T^4\cong 4T_\infty^3T-3T_\infty^4 \tag{8}$$

Using Eq. (8) into Eq. (7), we get

$$\frac{\partial q_r}{\partial y}=-\frac{16T_\infty^3\sigma^*}{3k^*}\frac{\partial^2 T}{\partial y^2} \tag{9}$$

Use Eq. (9) in Eq. (4), we obtain

$$\frac{\partial T}{\partial t}+u\frac{\partial T}{\partial x}+v\frac{\partial T}{\partial y}=\frac{k}{(\rho c)_f}\left(\frac{\partial^2 T}{\partial x^2}+\frac{\partial^2 T}{\partial y^2}\right)+\frac{1}{(\rho c)_f}\left(\frac{16T_\infty^3\sigma^*}{3k^*}\frac{\partial^2 T}{\partial y^2}\right)+\frac{\mu}{(\rho c)_f}\left(\frac{\partial u}{\partial y}\right)^2+\frac{Q}{(\rho c)_f}\left(T-T_\infty\right)+\frac{\sigma}{(\rho c)_f}(uB-E)^2+\tau\left\{D_B\left(\frac{\partial\varphi}{\partial x}\frac{\partial T}{\partial x}+\frac{\partial\varphi}{\partial y}\frac{\partial T}{\partial y}\right)+\frac{D_T}{T_\infty}\left[\left(\frac{\partial T}{\partial x}\right)^2+\left(\frac{\partial T}{\partial y}\right)^2\right]\right\} \tag{10}$$

Using the order of magnitude analysis for the y-direction momentum equation which is normal to the stretching sheet and boundary layer approximation (Daniel et al., 2017a; Ibrahim & Shankar, 2013), such as

$$\begin{aligned}&u\gg v\\&\frac{\partial u}{\partial y}\gg\frac{\partial u}{\partial x},\ \frac{\partial v}{\partial t},\ \frac{\partial v}{\partial x},\ \frac{\partial v}{\partial y}\\&\frac{\partial p}{\partial y}=0\end{aligned} \tag{11}$$

After the analysis, the boundary layer Eqs. (1)–(5) are reduced to the following as:

$$\frac{\partial u}{\partial x}+\frac{\partial v}{\partial y}=0 \tag{12}$$

$$\frac{\partial u}{\partial t}+u\frac{\partial u}{\partial x}+v\frac{\partial u}{\partial y}=\nu\left(\frac{\partial^2 u}{\partial y^2}\right)+\frac{\sigma}{\rho_f}\left(EB-B^2u\right)+\frac{1}{\rho_f}\left[\left(1-\varphi_\infty\right)\rho_{f\infty}\beta\left(T-T_\infty\right)-\left(\rho_p-\rho_{f\infty}\right)\beta\left(\varphi-\varphi_\infty\right)\right]g \tag{13}$$

$$\frac{\partial T}{\partial t}+u\frac{\partial T}{\partial x}+v\frac{\partial T}{\partial y}=\frac{k}{(\rho c)_f}\left(\frac{\partial^2 T}{\partial y^2}\right)+\frac{1}{(\rho c)_f}\left(\frac{16T_\infty^3\sigma^*}{3k^*}\frac{\partial^2 T}{\partial y^2}\right)+\frac{\mu}{(\rho c)_f}\left(\frac{\partial u}{\partial y}\right)^2+\frac{Q}{(\rho c)_f}(T-T_\infty)+\frac{\sigma}{(\rho c)_f}(uB-E)^2+\tau\left\{D_B\left(\frac{\partial \varphi}{\partial y}\frac{\partial T}{\partial y}\right)+\frac{D_T}{T_\infty}\left(\frac{\partial T}{\partial y}\right)^2\right\} \tag{14}$$

$$\frac{\partial \varphi}{\partial t}+u\frac{\partial \varphi}{\partial y}+v\frac{\partial \varphi}{\partial y}=D_B\left(\frac{\partial^2 \varphi}{\partial y^2}\right)+\frac{D_T}{T_\infty}\left(\frac{\partial^2 T}{\partial y^2}\right)-k_1(\varphi-\varphi_\infty) \tag{15}$$

The boundary conditions at the sheet are presented by

$$\begin{aligned} &y=0: \quad u=u_w(x,t), \quad v=v_w(x,t),\\ &T=T_W(x,t)=T_0+A_1x(1-at)^{-1},\\ &\varphi=\varphi_W(x,t)=\varphi_0+C_1x(1-at)^{-1},\\ &y\to\infty: \quad u\to 0, \quad T\to T_\infty=T_0+A_2x(1-at)^{-1},\\ &\varphi\to\varphi_\infty=\varphi_0+C_2x(1-at)^{-1} \end{aligned} \tag{16}$$

The equations are reduced into the dimensionless form by introducing the following dimensionless quantities defined as:

$$\psi=\sqrt{\frac{bv}{1-at}}xf(\eta), \quad \eta=y\sqrt{\frac{b}{v(1-at)}}, \quad \theta=\frac{T-T_\infty}{T_w-T_0}, \quad \phi=\frac{\varphi-\varphi_\infty}{\varphi_w-\varphi_0}, \tag{17}$$

The stream function ψ can be given as:

$$u=\frac{\partial \psi}{\partial y}, \quad v=-\frac{\partial \psi}{\partial x} \tag{18}$$

Using Eqs. (17) and (18) into Eqs. (12)–(16). The equations of momentum, energy and nanoparticle concentration in dimensionless form become:

$$f'''+ff''-f'^2-\delta\left(f'+\frac{\eta}{2}f''\right)+M\left(E_1-f'\right)+\lambda(\theta-Nr\phi)=0 \tag{19}$$

$$\frac{1}{Pr}\left(1+\frac{4}{3}Rd\right)\theta''+f\theta'-f'\theta-\delta\left(s_t+\frac{\eta}{2}\theta'+\theta\right)+Nb\phi'\theta'+Nt\theta'^2+Ec(f'')^2+MEc(f'+E_1)^2+\varepsilon\theta+s_tf'=0 \tag{20}$$

$$\phi''+Lef\phi'-Lef'\phi-Le\delta\left(s_c+\frac{\eta}{2}\phi'+\phi\right)+\frac{Nt}{Nb}\theta''-Le\gamma\phi-Les_cf'=0 \tag{21}$$

The boundary conditions are given by

$$\begin{aligned} &f=s, \quad f'=1, \quad \theta=1-s_t, \quad \phi=1-s_c, \quad \text{at} \quad \eta=0\\ &f'=0, \quad \theta=0, \quad \phi=0, \quad \text{as} \quad \eta\to\infty \end{aligned} \tag{22}$$

here f',θ and ϕ is the dimensionless velocity, temperature, and concentration, respectively, $\delta=a/b$ represent the unsteadiness parameter, $\lambda=Gr/Re^2$ is the mixed convection parameter (Richardson number) for values of ($\lambda>0$) associate to heated surface and ($\lambda<0$) corresponds to cold surface whereas ($\lambda=0$) indicates forced convection flow, $Gr=g\beta(1-\varphi_\infty)(T_W-T_0)\rho_{f\infty}/\nu^2\rho_f$ is the Grashof number, $Re=u_wx/v$ is the Reynolds number, $Nr=(\rho_f-\rho_{f\infty})(\varphi_W-\varphi_0)/\beta\rho_{f\infty}(1-\varphi_\infty)(T_W-T_0)$ is the buoyancy ratio parameter, $Pr=v/\alpha$ stand for Prandtl number, $Nb=(\rho c)_pD_B(\varphi_w-\varphi_\infty)/(\rho c)_fv$ is the Brownian motion parameter, $Le=v/D_B$ is the Lewis, $Nt=(\rho c)_pD_T(T_w-T_\infty)/(\rho c)_fvT_\infty$ is the thermophoresis parameter, $M=\sigma B_0^2/b\rho_f$ is the magnetic field parameter, $E_1=E_0/u_WB_0$ is the electric field parameter, $Ec=u_W^2/c_p(T_w-T_\infty)$ is the Eckert number, $s_t=A_2/A_1$ denote the thermal stratification parameter, $s_c=C_2/C_1$ indicate the concentration stratification parameter, $s=v_0/\sqrt{vb}$ is the suction ($s>0$)/injection ($s<0$) parameter and $Rd=4\sigma^*T_\infty^3/k^*k$ is the radiation parameter, $\varepsilon=Q_0/b(\rho c)_f$ is the heat generation/absorption as ($\varepsilon>0$) denotes heat generation and ($\varepsilon<0$) denotes heat absorption, $\gamma=k_0/b$ is the chemical reaction, for ($\gamma>0$) associates to destructive chemical reaction while ($\gamma<0$) corresponds to generative chemical reaction respectively. Where prime represents differentiation with respect to η. In our present study, the selection of non-dimensional physical sundry parameters of nanofluids is considered to vary in view of the works of (Abolbashari et al., 2014; Daniel, Aziz, Ismail, & Salah, 2017d; Daniel, Aziz, Ismail, & Salah, 2017e; Hsiao, 2016, 2017; Ibrahim & Shankar, 2013; Mabood et al., 2015; Noghrehabadi, Saffarian, Pourrajab, & Ghalambaz, 2013).

The skin friction coefficient the local Nusselt number and the local Sherwood number are

$$c_f=\frac{\tau_w}{\rho u_w^2(x,t)}, \quad Nu=\frac{xq_w}{k(T_w-T_\infty)}, \quad Sh=\frac{xq_m}{D_B(\varphi_w-\varphi_\infty)}, \tag{23}$$

where

$$q_w=-\left(\left(k+\frac{16\sigma^*T_\infty^3}{3k^*}\right)\frac{\partial T}{\partial y}\right)_{y=0}, \quad q_m=-D_B\left(\frac{\partial \varphi}{\partial y}\right)_{y=0}, \quad \tau_w=\mu_f\left(\frac{\partial u}{\partial y}\right)_{y=0}, \tag{24}$$

here τ_w is the shear stress in the stretching surface, q_w is the surface heat flux while q_m is the surface mass flux, $Re=u_wx/v$ is the Reynolds number and k is the thermal conductivity of the nanofluid. For the local skin-friction coefficient, local Nusselt

Table 1
Comparison with previously published works for the values of skin friction coefficient $-f''(0)$ for various values of M, s, and δ when $E_1 = Nr = \lambda = 0$.

M	s	δ	Khan and Azam (2017)	Ibrahim and Shankar (2013)	Hayat et al. (2016a)	Present results
0.0	0.0	0.0	–	1.0000	–	1.000000
	0.5		–	1.2808	1.2808	1.280776
0.5	0.5		–	1.5000	–	1.500000
1.0	0.5		–	1.6861	–	1.686141
1.5	0.5		–	1.8508	–	1.850781
2.5	0.5		–	2.0000	–	2.000000
1.0	0.0		–	1.4142	1.4142	1.414214
5.0			–	–	2.4494	2.449490
0.0		0.0	1.0000	–	–	1.000000
		0.2	1.06801	–	–	1.068012
		0.4	1.13469	–	–	1.134685
		0.6	1.19912	–	–	1.199117
		0.8	1.26104	–	–	1.261040
		1.2	1.37772	–	–	1.377720
		1.4	1.43284	–	–	1.432831
		2.0	1.58737	–	–	1.587358

and local Sherwood numbers are presented in non-dimensional form as

$$Re^{1/2} c_f = f''(0),$$
$$Nu/Re^{1/2} = -\left(1 + \frac{4}{3}Rd\right)\left(\frac{1}{1 - s_t}\right)\theta'(0) \tag{25}$$
$$Sh/Re^{1/2} = -\left(\frac{1}{1 - s_c}\right)\phi'(0)$$

3. Results and discussion

In this paper, the transformed equations momentum, energy and concentration (19)–(21) subjected to the boundary condition (22) are solved numerically by an efficient implicit finite difference scheme known as Keller box method which is discussed comprehensively in (Cebeci & Bradshaw, 2012). The computational analysis is performed with sundry parameters viz Prandtl number Pr, magnetic field M, electric field E_1, unsteadiness parameter δ, mixed convection parameter λ, buoyancy ratio parameter Nr, suction/injection s, thermal radiation parameter Rd, Brownian motion Nb, thermophoresis Nt, Eckert number Ec, heat generation/absorption ε, thermal stratification s_t, Lewis number Le, chemical reaction γ, and concentration stratification s_c. We have selected a step size of $\Delta\eta = 0.01$ to satisfy the convergence condition of 10^{-5}. In Table 1, we see that the present computational scheme from the numerical values reveals is in an excellent agreement with the results reported by previous studies such as (Hayat, Imtiaz, & Alsaedi, 2016a; Ibrahim & Shankar, 2013; Khan & Azam, 2017), under limiting conditions. Table 2 displays the numerical values of local Nusselt and Sherwood numbers for different values of s, Le, Nt, Nb, s_t, s_c, Ec, E_1, M, Rd, δ, ε, γ, Nr, and λ when $Pr = 6.2$ are conducted. From this table, it is examined that the values of local Nusselt number are increased by increasing the values of s, s_c, E_1, δ, and λ but these decrease by increasing Le, Nt, Nb, s_t, Ec, M, Rd, ε, γ, and Nr.

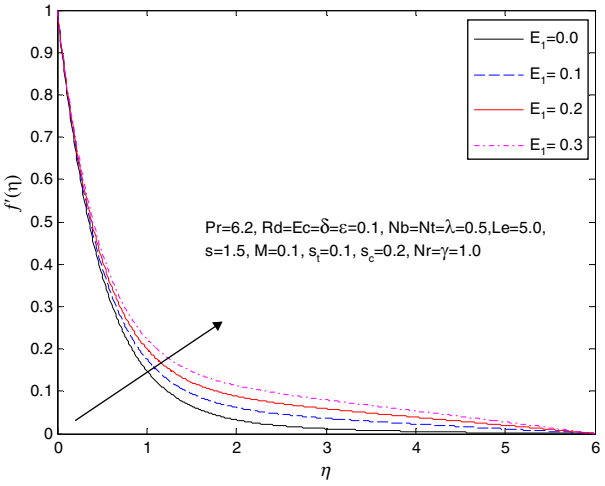

Fig. 2. Influence of E_1 on the velocity profile $f'(\eta)$.

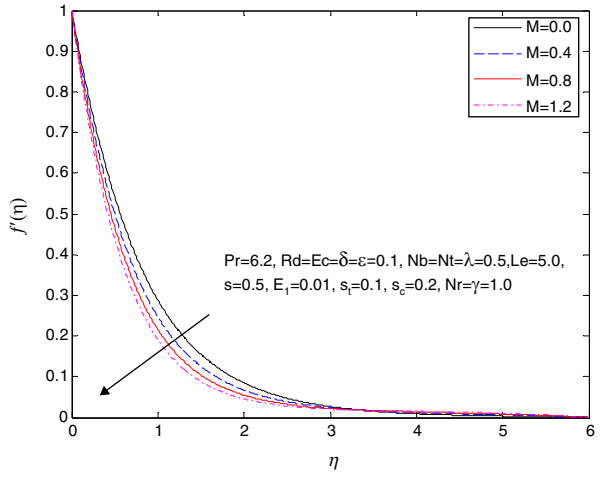

Fig. 3. Influence of M on the velocity profile $f'(\eta)$.

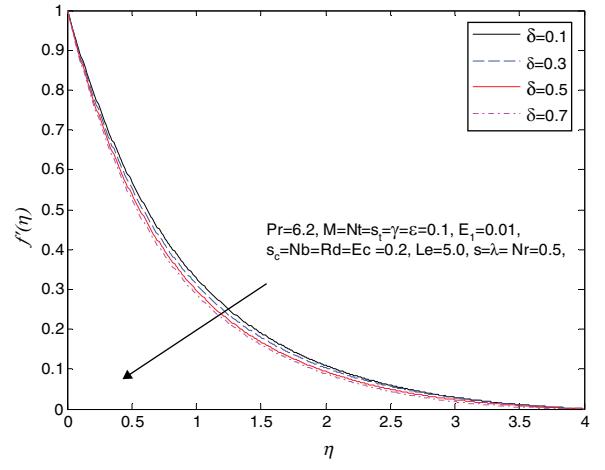

Fig. 4. Influence of δ on the velocity profile $f'(\eta)$.

The values of local Sherwood numbers increase by increasing the values of s, Le, Nt, Nb, Ec, E_1, M, Rd, δ, ε, γ, and λ whereas its decreases with increases in the values of s_t, s_c, and Nr. The results obtained are shown through Figures 2–20 for the velocity,

Table 2
Numerical results of local Nusselt number $Nu_x/Re^{1/2}$ and local Sherwood number $Sh_x/Re^{1/2}$ for various values of s, Le, Nt, Nb S_t, S_c, Ec, E_1, M, Rd, δ, λ, Nr, ε and γ when $Pr = 6.2$.

s	Le	Nt	Nb	S_t	S_c	Ec	E_1	M	Rd	δ	ε	γ	Nr	λ	$Nu/Re^{1/2}$	$Sh/Re^{1/2}$
0.1	5.0	0.1	0.2	0.1	0.2	0.2	0.1	0.1	0.2	0.1	0.1	1.0	0.1	0.5	1.609856	3.277781
0.3															1.914229	3.684784
0.5															2.260243	4.104724
0.1	2.0														1.836066	1.696388
	4.0														1.662801	2.828166
	7.0														1.533674	4.057326
	5.0	0.2													1.424676	3.212881
		0.3													1.276608	3.214053
		0.5													1.061147	3.305251
		0.1	0.1												1.983094	2.809780
			0.3												1.308123	3.412765
			0.5												0.875038	3.491720
			0.2	0.2											1.554430	3.230745
				0.4											1.465419	3.154099
				0.5											1.449703	3.138346
				0.1	0.1										1.516611	3.451757
					0.4										1.640436	2.840690
					0.5										1.683675	2.636516
					0.2	0.1									1.616170	3.231450
						0.3									1.498383	3.264895
						0.5									1.383440	3.297314
						0.2	0.2								1.567688	3.250943
							0.5								1.589580	3.258948
							1.0								1.595010	3.273710
							0.1	0.2							1.533827	3.250854
								0.5							1.464559	3.258183
								1.0							1.352284	3.270999
								0.1	0.3						1.529815	3.250125
									0.5						1.475525	3.255883
									0.7						1.423302	3.262969
									1.0	0.2					1.400481	3.383713
										0.4					1.482374	3.588870
										0.7					1.586703	3.865858
										0.1	0.2				1.302533	3.291501
											0.3				1.255259	3.309122
											0.5				1.176202	3.345212
											0.1	1.5			1.343690	3.524437
												2.0			1.336748	3.761108
												2.5			1.330360	3.984570
												1.0	0.3		1.334108	3.267329
													0.5		1.315966	3.260383
													1.0		1.263585	3.242419
													0.1	1.0	1.430948	3.315061
														1.5	1.483361	3.356874
														2.0	1.515111	3.400111

temperature, and nanoparticle concentration profiles for sundry parameters respectively.

Figures 2–7 display the velocity profiles $f'(\eta)$ for the various embedded parameters viz electric field, magnetic field, unsteadiness parameter, mixed convection parameter, buoyancy ratio parameter, and suction/injection parameter. Figure 2 indicates that higher values of electric parameter increase the nanofluid velocity. An electric parameter acts as accelerating force. The higher electric parameter has the stronger Lorentz force and the lower electric parameter associated with the weaker Lorentz force. The stronger Lorentz force creates more enhancement and resolves sticky effect due to the nanoparticles in the fluid that signified an increase in the convective heat transfer and momentum boundary layer thickness. The effect of magnetic field parameter M on the nanofluid velocity profile is exhibited in Figure 3. The velocity and momentum boundary layer thickness decreased for higher values of the magnetic parameter. Magnetic field results in a resistive type force known as Lorentz flow where it opposite the flow. This leads to resists in the fluid flow behavior that amount to a reduction in the velocity and thinner boundary layer thickness. Figure 4 demonstrates the effect of unsteadiness parameter δ on the nanofluid velocity profile. The behavior is due to acceleration case ($\delta > 0$), a lower rate of fluid flow and thinner momentum boundary layer thickness. The velocity profile reduces for the higher acceleration. In Figure 5, it is noticed that the momentum

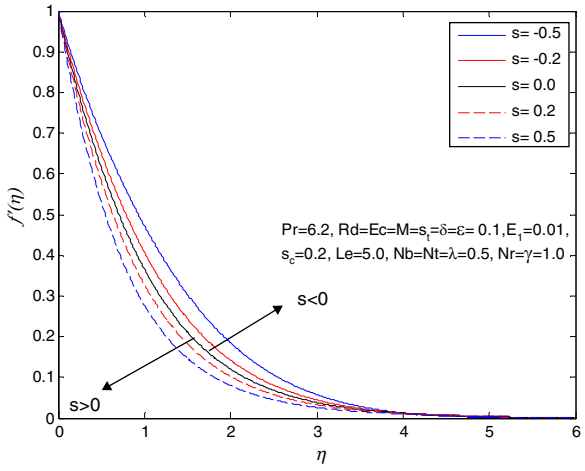

Fig. 5. Influence of s on the velocity profile $f'(\eta)$.

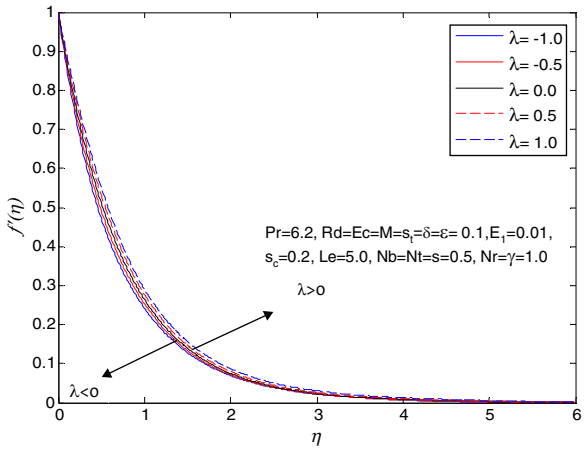

Fig. 6. Influence of λ on the velocity profile $f'(\eta)$.

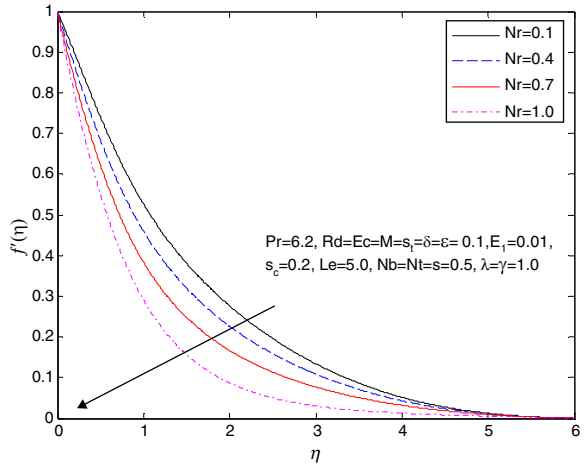

Fig. 7. Influence of Nr on the velocity profile $f'(\eta)$.

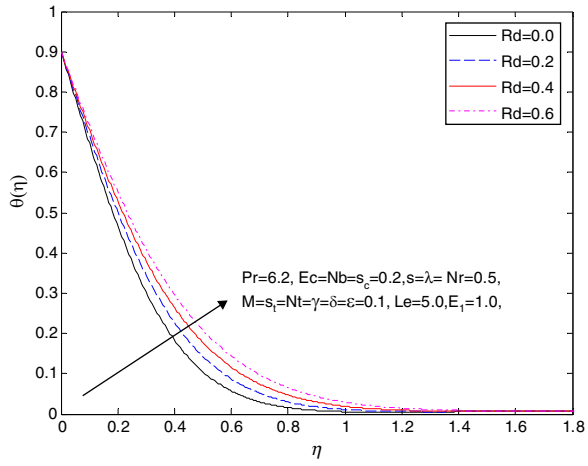

Fig. 8. Influence of Rd on the temperature profile $\theta(\eta)$.

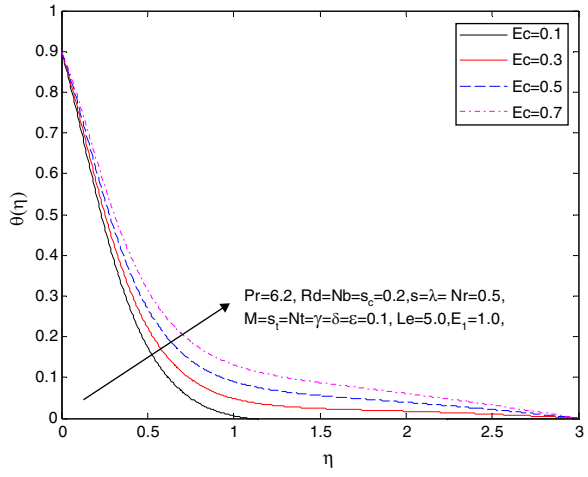

Fig. 9. Influence of Ec on the temperature profile $\theta(\eta)$.

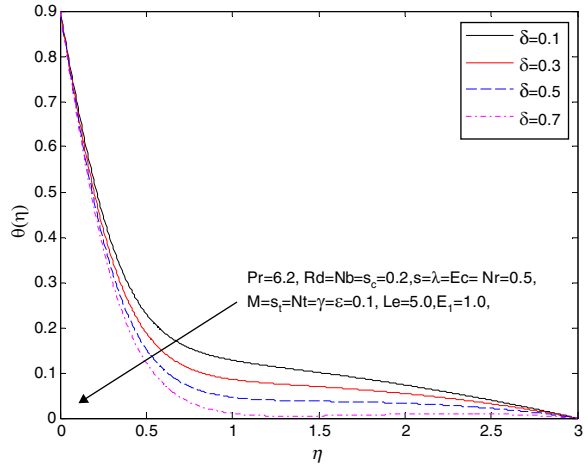

Fig. 10. Influence of δ on the temperature profile $\theta(\eta)$.

boundary layer thickness for the nanofluid decreases with increasing the values of the suction parameter ($s > 0$). This can be attributed to a decrease in the fluid velocity due to increasing nanofluid suction at the stretching surface. While reverse behavior occurred for injection parameter ($s < 0$). The effect of mixed convection parameter λ on the nanofluid velocity is presented in Figure 6. Corresponds to heated surface ($\lambda > 0$), higher values leads to enhancement in the fluid velocity and

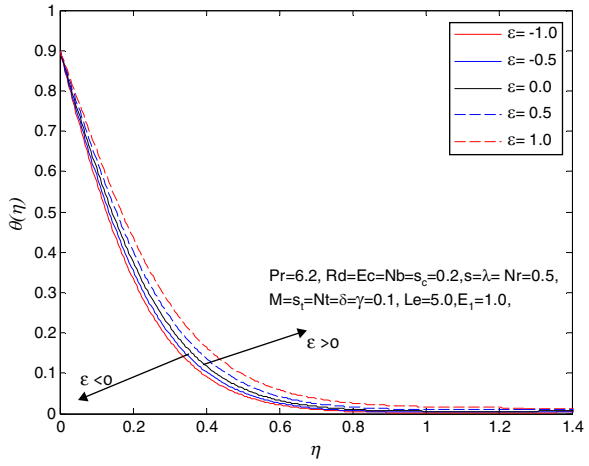

Fig. 11. Influence of ε on the temperature profile $\theta(\eta)$.

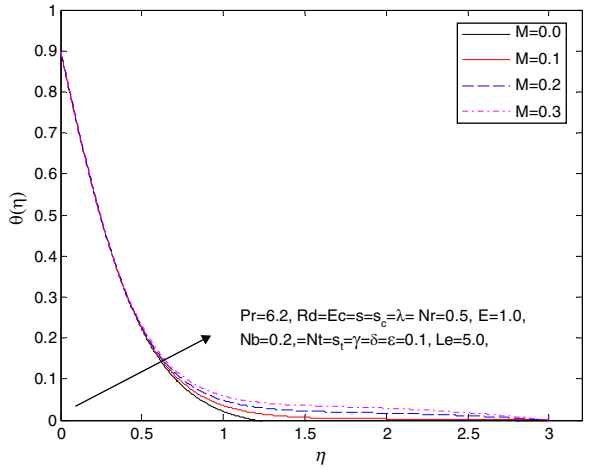

Fig. 12. Influence of M on the temperature profile $\theta(\eta)$.

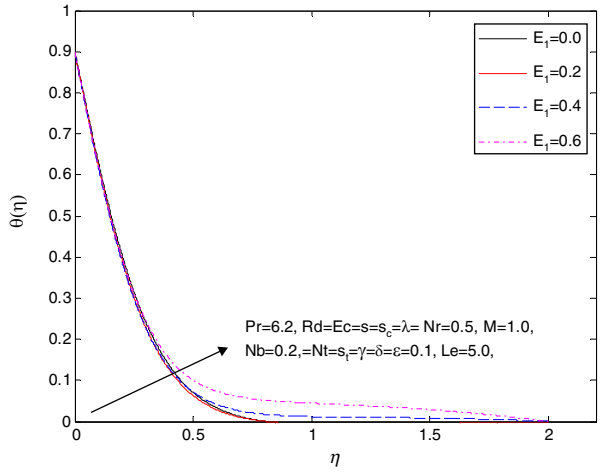

Fig. 13. Influence of E_1 on the temperature profile $\theta(\eta)$.

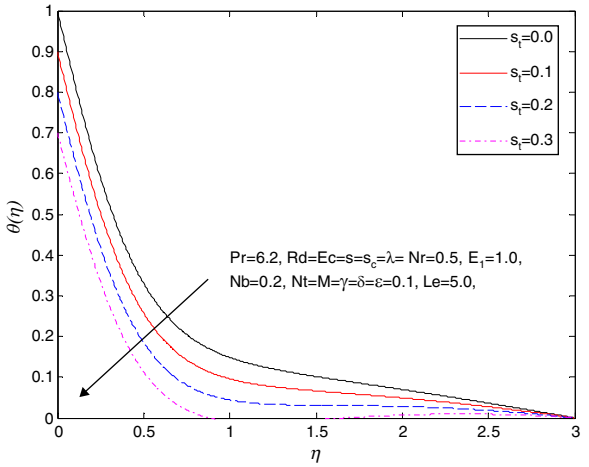

Fig. 14. Influence of s_t on the temperature profile $\theta(\eta)$.

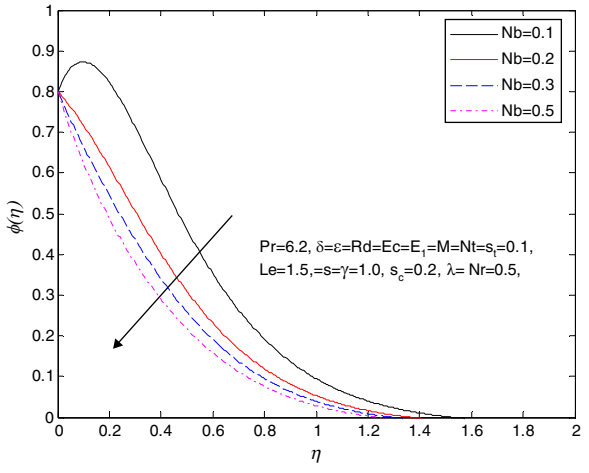

Fig. 15. Influence of Nb on the concentration profile $\phi(\eta)$.

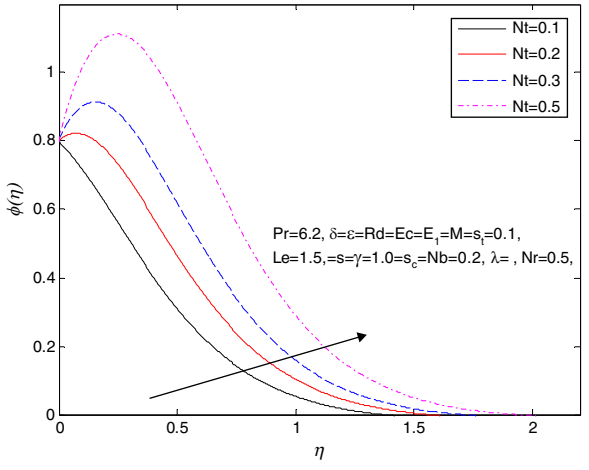

Fig. 16. Influence of Nt on the concentration profile $\phi(\eta)$.

thicker momentum boundary layer thickness. This leads to assist the nanofluid flow in the upward direction, whereas ($\lambda < 0$) indicate cold surface opposing the nanofluid flow in the downward direction with thinner momentum boundary layer thickness. As ($\lambda = 0$) signifies absence of the mixed convection, therefore force convection behavior due to nanofluid velocity. The effect of buoyancy ratio parameter Nr on the nanofluid velocity is publicized in Figure 7. It is noticed that the nanofluid velocity reduces with a high amount of buoyancy force. The

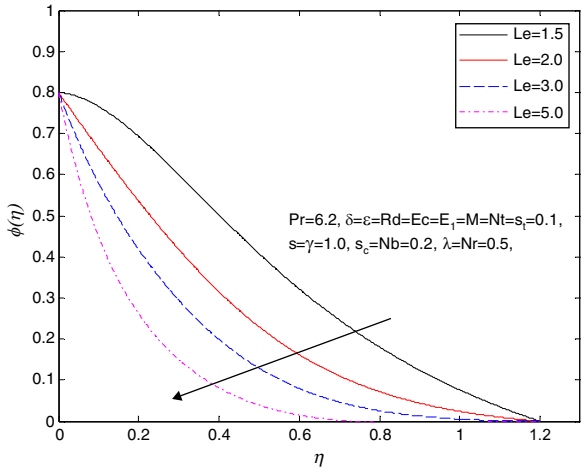

Fig. 17. Influence of Le on the concentration profile $\phi(\eta)$.

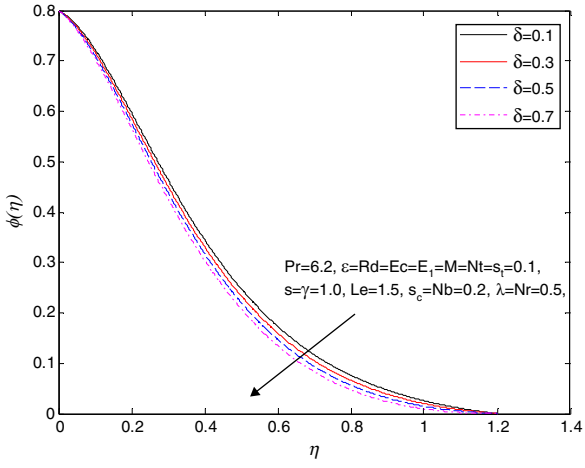

Fig. 18. Influence of δ on the concentration profile $\phi(\eta)$.

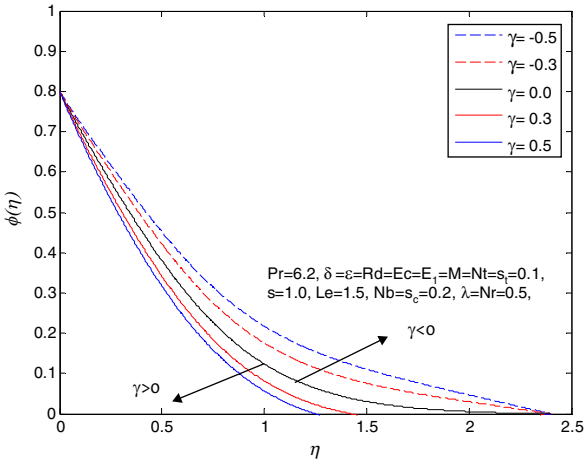

Fig. 19. Influence of γ on the concentration profile $\phi(\eta)$.

buoyancy force behaves as unfavorable pressure gradient, therefore, stronger buoyancy force reduced the fluid flow due to stretching surface in the downwind direction and thinner momentum boundary layer thickness.

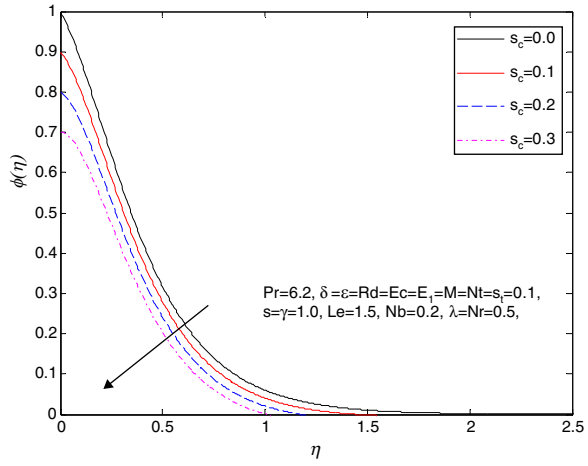

Fig. 20. Influence of S_c on the concentration profile $\phi(\eta)$.

In Figures 8–14 display the effects of thermal radiation Rd, Eckert number Ec, unsteadiness parameter δ, heat generation/absorption parameter ε, magnetic field parameter M, electric field parameter E_1, and thermal stratification parameter s_t on the temperature profiles $\theta(\eta)$. Figure 8 elucidates the changes that are noticed in nanofluid temperature profiles due to increase in the values of thermal radiation parameter Rd. It is worth noticing that the nanofluid temperature increases as thermal radiation increase due to the fact that the conduction impact of the nanofluid improves in the presence of thermal radiation. Hence higher values of radiation parameter mean higher surface heat flux and so, enhance the temperature within the boundary layer region. It is also demonstrated that thermal boundary layer thickness increases with increasing the values of thermal radiation. In Figure 9, illuminates that the nanofluid temperature and thermal boundary layer thickness are enhanced due to kinetic increase rises over the energy to enthalpy with an increase in the values of Eckert number. The influence of unsteadiness parameter on the temperature profile in Figure 10, is similar to of the velocity in Figure 4. The effect of heat generation/absorption on the temperature is depicted in Figure 11. It is noted that heat source ($\varepsilon > 0$) gives an increase in the temperature of the fluid and the thermal boundary layer thickness. While as the heat sink ($\varepsilon < 0$) provides a decrease in the temperature of the fluid and thinner thermal boundary layer thickness. For $\varepsilon = 0$ signify the absence of heat generation/absorption. Figure 12 establishes the impact of magnetic field parameter M on the nanofluid temperature profiles. The transverse magnetic field has increased the thermal boundary layer thickness. Thus, an enhancement in thermal boundary layer thickness and fluid temperature. The magnetic field performances as a strong Lorentz force that boost on the nanofluid temperature in the boundary region. The effect of the electric field parameter E_1 on the temperature profile $\theta(\eta)$ is revealed in Figure 13. The electric field behaves as accelerating force that enhances the fluid temperature and thermal boundary layer thickness. A higher value of an electric field is associated with thicker higher amount temperature distribution within the boundary layer region of the vicinity of the nanofluid. Figure 14 is a sketch for nanofluid

temperature profile with various values of thermal stratification parameter s_t. The nanofluid temperature is reduced for higher values of thermal stratification parameter. It is also noticed that the case of prescribed surface temperature is achieved when thermal stratification is absence ($s_t = 0$). Physically, the variation between the surface temperature and the ambient temperature is diminished for a high amount of thermal stratification. Consequently, leads lower amount of fluid temperature in the boundary region of the nanofluid and thinner thermal boundary layer thickness.

The effects of Brownian motion parameter Nb, thermophoresis parameter Nt, Lewis number Le, unsteadiness parameter δ, chemical reaction parameter γ, and concentration stratification parameter s_c on the concentration profiles $\phi(\eta)$ are shown in Figures 15–20. In Figure 15 portrays the influence of Brownian motion parameter on the nanoparticle concentration profiles. It is noticed that the nanoparticle concentration of the nanofluid reduced with increase in Brownian motion of the nanoparticles. It is worth interesting to note that Brownian motion of the nanoparticles at the molecular and nanosized rates is a key nanoscale processes governing their thermal behavior with the fluid molecules. Consequently, leads to thinner solutal thermal boundary layer thickness due to Brownian motion. Figure 16 proves the effect of thermophoresis parameter on the concentration profiles $\phi(\eta)$. The impact of the thermophoresis parameter on the nanoparticles concentration distribution is monotonic meaning the nanoparticles concentration is sensitive to increases in thermophoresis parameter. The magnitude of the concentration gradient at the surface decrease for higher values of thermophoresis parameter. Hence, due to the fact that as a thermophoresis depreciated mass transfer of nanofluids. In Figure 17 examines the influence of Lewis number on the nanoparticles concentration. It is worth noticeable that the nanoparticles concentration is reduced significantly for higher values of Lewis number. This reduction in nanoparticles concentration is due to the change in Brownian motion coefficient. Higher values of Lewis number associated to feebler Brownian diffusion coefficient. Figure 18 demonstrates the behavior of unsteadiness parameter on the concentration profiles, which is similar to that of Figure 10. In Figure 19 elucidates the effect of chemical reaction on the nanoparticles concentration profile. It is of interest to note that nanoparticles concentration enhances for higher values of destructive chemical reaction parameter ($\gamma < 0$). Whereas reverse behavior occurred for generative chemical reaction parameter ($\gamma > 0$). Perhaps, higher values of generative chemical reaction associated with the high rate of generative chemical reaction which generates the fluid species more efficiently and thus nanoparticles concentration rises. But opposite trend is noticed for destructive chemical reaction parameter ($\gamma < 0$). For ($\gamma = 0$) implies absence of chemical reaction. The influence of concentration stratification on the nanoparticle concentration is described in Figure 20. An increase in concentration stratification parameter leads to a decrease in nanoparticles concentration and solutal concentration boundary layer thickness. This is as result of the fact that fluid near the plate can have a concentration lower than the ambient medium. The nanoparticles concentration is maximum at ($s_c = 0$).

4. Final remarks

In this work, unsteady mixed convection with the combined effects of thermal radiation, heat generation/absorption and chemical reaction on the electrical magnetohydrodynamic (MHD) flow of nanofluid in the presence viscous dissipation and Joule heating over a permeable stretching sheet is investigated numerically. Buongiorno model was used to incorporate the effects of Brownian motion and thermophoresis. The boundary layer governing equations are converted to nonlinear ordinary differential equations using similarity transformations and then solved numerically with implicit finite difference scheme. On the basis of findings with sundry parameters in this work, we drew the following main conclusions:

1. Velocity and temperature increase with an increase in an electric parameter.
2. Thermal radiation and viscous dissipation increase the temperature profiles.
3. Heat source increases the temperature while as reverse occurred with a heat sink.
4. Destructive chemical reaction enhances the nanoparticles concentration while opposite behave happened in the case of a generative chemical reaction.
5. Reversed behavior occurred with Brownian motion and thermophoresis parameter with nanoparticles concentration.
6. Thermal stratification reduced the temperature profile and concentration stratification decreased the nanoparticles concentration profile.
7. Buoyancy ratio parameter decreases both Nusselt and Sherwood numbers whereas mixed convection parameter increase both for higher values.
8. The skin friction, local Nusselt and Sherwood number are sensitive to increase in suction whereas, higher values unsteadiness parameter reduces the velocity, temperature, and nanoparticles concentration profile.

Conflict of interest

The authors have no conflicts of interest to declare.

Acknowledgment

The authors would like to acknowledge Ministry of Higher Education and Research Management Centre, UTM for the financial support through GUP with vote number 11H90, Flagship groups with vote numbers 03G50 and 03G53 for this research.

References

Abolbashari, M. H., Freidoonimehr, N., Nazari, F., & Rashidi, M. M. (2014). Entropy analysis for an unsteady MHD flow past a stretching permeable surface in nano-fluid. *Powder Technology*, *267*, 256–267.

Bég, O. A., Khan, M. S., Karim, I., Alam, M. M., & Ferdows, M. (2014). Explicit numerical study of unsteady hydromagnetic mixed convective nanofluid flow from an exponentially stretching sheet in porous media. *Applied Nanoscience*, *4*(8), 943–957.

Bhatti, M., Zeeshan, A., Ijaz, N., Bég, O. A., & Kadir, A. (2016). Mathematical modelling of nonlinear thermal radiation effects on EMHD peristaltic pumping of viscoelastic dusty fluid through a porous medium duct. *Engineering Science and Technology: An International Journal*, *20*(3), 1129–1139.

Buongiorno, J. (2006). Convective transport in nanofluids. *Journal of Heat Transfer*, *128*(3), 240–250.

Cebeci, T., & Bradshaw, P. (2012). *Physical and computational aspects of convective heat transfer*. Springer Science & Business Media.

Choi, S. (1995). Enhancing conductivity of fluids with nanoparticles. *ASME Fluids Engineering Division*, *231*, 99–105.

Daniel, Y. S. (2015a). Presence of heat generation/absorption on boundary layer slip flow of nanofluid over a porous stretching sheet. *American Journal of Heat and Mass Transfer*, *2*(1), 15.

Daniel, Y. S. (2015b). Steady MHD laminar flows and heat transfer adjacent to porous stretching sheets using HAM. *American Journal of Heat and Mass Transfer*, *2*(3), 146–159.

Daniel, Y. S. (2016). Laminar convective boundary layer slip flow over a flat plate using homotopy analysis method. *Journal of The Institution of Engineers (India): Series E*, *97*(2), 115–121.

Daniel, Y. S. (2017). MHD laminar flows and heat transfer adjacent to permeable stretching sheets with partial slip condition. *Journal of Advanced Mechanical Engineering*, *4*(1), 1–15.

Daniel, Y. S., & Daniel, S. K. (2015). Effects of buoyancy and thermal radiation on MHD flow over a stretching porous sheet using homotopy analysis method. *Alexandria Engineering Journal*, *54*(3), 705–712.

Daniel, Y. S., Aziz, Z. A., Ismail, Z., & Salah, F. (2017a). Effects of slip and convective conditions on MHD flow of nanofluid over a porous nonlinear stretching/shrinking sheet. *Australian Journal of Mechanical Engineering*, 1–17.

Daniel, Y. S., Aziz, Z. A., Ismail, Z., & Salah, F. (2017b). Effects of thermal radiation, viscous and Joule heating on electrical MHD nanofluid with double stratification. *Chinese Journal of Physics*, *55*(3), 630–651.

Daniel, Y. S., Aziz, Z. A., Ismail, Z., & Salah, F. (2017c). Entropy analysis in electrical magnetohydrodynamic (MHD) flow of nanofluid with effects of thermal radiation, viscous dissipation, and chemical reaction. *Theoretical and Applied Mechanics Letters*, http://dx.doi.org/10.1016/j.taml.2017.06.003

Daniel, Y. S., Aziz, Z. A., Ismail, Z., & Salah, F. (2017d). Impact of thermal radiation on electrical MHD flow of nanofluid over nonlinear stretching sheet with variable thickness. *Alexandria Engineering Journal*, http://dx.doi.org/10.1016/j.aej.2017.07.007

Daniel, Y. S., Aziz, Z. A., Ismail, Z., & Salah, F. (2017e). Numerical study of Entropy analysis for electrical unsteady natural magnetohydrodynamic flow of nanofluid and heat transfer. *Chinese Journal of Physics*, *55*(5), 1821–1848.

Freidoonimehr, N., Rashidi, M. M., & Mahmud, S. (2015). Unsteady MHD free convective flow past a permeable stretching vertical surface in a nano-fluid. *International Journal of Thermal Sciences*, *87*, 136–145.

Gómez-Pastora, J., Dominguez, S., Bringas, E., Rivero, M. J., Ortiz, I., & Dionysiou, D. D. (2017). Review and perspectives on the use of magnetic nanophotocatalysts (MNPCs) in water treatment. *Chemical Engineering Journal*, *310*, 407–427.

Hayat, T., & Qasim, M. (2011). Radiation and magnetic field effects on the unsteady mixed convection flow of a second grade fluid over a vertical stretching sheet. *International Journal for Numerical Methods in Fluids*, *66*(7), 820–832.

Hayat, T., Gull, N., Farooq, M., & Ahmad, B. (2015). Thermal radiation effect in MHD flow of Powell–Eyring nanofluid induced by a stretching cylinder. *Journal of Aerospace Engineering*, *29*(1), 04015011.

Hayat, T., Imtiaz, M., & Alsaedi, A. (2016). Unsteady flow of nanofluid with double stratification and magnetohydrodynamics. *International Journal of Heat and Mass Transfer*, *92*, 100–109.

Hayat, T., Muhammad, T., Shehzad, S., & Alsaedi, A. (2016). Modeling and analysis for hydromagnetic three-dimensional flow of second grade nanofluid. *Journal of Molecular Liquids*, *221*, 93–101.

Hayat, T., Qayyum, S., Waqas, M., & Alsaedi, A. (2016). Thermally radiative stagnation point flow of Maxwell nanofluid due to unsteady convectively heated stretched surface. *Journal of Molecular Liquids*, *224*, 801–810.

Hayat, T., Waqas, M., Khan, M. I., & Alsaedi, A. (2016). Analysis of thixotropic nanomaterial in a doubly stratified medium considering magnetic field effects. *International Journal of Heat and Mass Transfer*, *102*, 1123–1129.

Hayat, T., Waqas, M., Shehzad, S., & Alsaedi, A. (2016). On 2D stratified flow of an Oldroyd-B fluid with chemical reaction: An application of non-Fourier heat flux theory. *Journal of Molecular Liquids*, *223*, 566–571.

Hayat, T., Mumtaz, M., Shafiq, A., & Alsaedi, A. (2017). Stratified magnetohydrodynamic flow of tangent hyperbolic nanofluid induced by inclined sheet. *Applied Mathematics and Mechanics*, *38*(2), 271–288.

Hayat, T., Waqas, M., Khan, M. I., & Alsaedi, A. (2017). Impacts of constructive and destructive chemical reactions in magnetohydrodynamic (MHD) flow of Jeffrey liquid due to nonlinear radially stretched surface. *Journal of Molecular Liquids*, *225*, 302–310.

Hedayatnasab, Z., Abnisa, F., & Daud, W. M. A. W. (2017). Review on magnetic nanoparticles for magnetic nanofluid hyperthermia application. *Materials & Design*, *123*, 174–196.

Hsiao, K.-L. (2016). Stagnation electrical MHD nanofluid mixed convection with slip boundary on a stretching sheet. *Applied Thermal Engineering*, *98*, 850–861.

Hsiao, K.-L. (2017). Combined electrical MHD heat transfer thermal extrusion system using Maxwell fluid with radiative and viscous dissipation effects. *Applied Thermal Engineering*, *112*, 1281–1288.

Hussain, S. (2017). Finite element solution for MHD flow of nanofluids with heat and mass transfer through a porous media with thermal radiation, viscous dissipation and chemical reaction effects. *Advances in Applied Mathematics and Mechanics*, *9*(4), 904–923.

Ibrahim, W., & Shankar, B. (2013). MHD boundary layer flow and heat transfer of a nanofluid past a permeable stretching sheet with velocity, thermal and solutal slip boundary conditions. *Computers & Fluids*, *75*, 1–10.

Jing, D., Pan, Y., & Wang, X. (2017). Joule heating, viscous dissipation and convective heat transfer of pressure-driven flow in a microchannel with surface charge-dependent slip. *International Journal of Heat and Mass Transfer*, *108*, 1305–1313.

Khan, M., & Azam, M. (2017). Unsteady heat and mass transfer mechanisms in MHD Carreau nanofluid flow. *Journal of Molecular Liquids*, *225*, 554–562.

Khan, M. I., Tamoor, M., Hayat, T., & Alsaedi, A. (2017). MHD boundary layer thermal slip flow by nonlinearly stretching cylinder with suction/blowing and radiation. *Results in Physics*, *7*, 1207–1211.

Kumar, R., & Sood, S. (2017). Combined influence of fluctuations in the temperature and stretching velocity of the sheet on MHD flow of Cu-water nanofluid through rotating porous medium with cubic auto-catalysis chemical reaction. *Journal of Molecular Liquids*, *237*, 347–360.

Lin, Y., Zheng, L., Zhang, X., Ma, L., & Chen, G. (2015). MHD pseudo-plastic nanofluid unsteady flow and heat transfer in a finite thin film over stretching surface with internal heat generation. *International Journal of Heat and Mass Transfer*, *84*, 903–911.

Mabood, F., & Khan, W. (2016). Analytical study for unsteady nanofluid MHD Flow impinging on heated stretching sheet. *Journal of Molecular Liquids*, *219*, 216–223.

Mabood, F., Khan, W., & Ismail, A. M. (2015). MHD boundary layer flow and heat transfer of nanofluids over a nonlinear stretching sheet: A numerical study. *Journal of Magnetism and Magnetic Materials*, *374*, 569–576.

Malvandi, A., Hedayati, F., & Ganji, D. (2014). Slip effects on unsteady stagnation point flow of a nanofluid over a stretching sheet. *Powder Technology*, *253*, 377–384.

Mehmood, K., Hussain, S., & Sagheer, M. (2016). Mixed convection flow with non-uniform heat source/sink in a doubly stratified magnetonanofluid. *AIP Advances*, *6*(6), 065126.

Mohammed, L., Gomaa, H. G., Ragab, D., & Zhu, J. (2017). Magnetic nanoparticles for environmental and biomedical applications: A review. *Particuology*, *30*, 1–14.

Noghrehabadi, A., Saffarian, M. R., Pourrajab, R., & Ghalambaz, M. (2013). Entropy analysis for nanofluid flow over a stretching sheet in the presence of heat generation/absorption and partial slip. *Journal of Mechanical Science and Technology*, *27*(3), 927–937.

Pal, D., & Mandal, G. (2016). Thermal radiation and MHD effects on boundary layer flow of micropolar nanofluid past a stretching sheet with

non-uniform heat source/sink. *International Journal of Mechanical Sciences*, *126*, 308–318.

Ramzan, M., Bilal, M., & Chung, J. D. (2017). Radiative flow of Powell–Eyring magneto-Nanofluid over a stretching cylinder with chemical reaction and double stratification near a stagnation point. *PLOS ONE*, *12*(1), e0170790.

Rehman, K. U., Malik, M., Salahuddin, T., & Naseer, M. (2016). Dual stratified mixed convection flow of Eyring–Powell fluid over an inclined stretching cylinder with heat generation/absorption effect. *AIP Advances*, *6*(7), 075112.

Sandeep, N., & Sulochana, C. (2015). Dual solutions for unsteady mixed convection flow of MHD micropolar fluid over a stretching/shrinking sheet with non-uniform heat source/sink. *Engineering Science and Technology: An International Journal*, *18*(4), 738–745.

Shagaiy, Y., Aziz, Z. A., Ismail, Z., & Salah, F. (2017). Effects of thermal radiation, viscous and Joule heating on electrical MHD Nanofluid with double stratification. *Chinese Journal of Physics*, *55*(3), 630–651.

Shateyi, S., & Motsa, S. (2011). Boundary layer flow and double diffusion over an unsteady stretching surface with Hall effect. *Chemical Engineering Communications*, *198*(12), 1545–1565.

Sparrow, E., & Cess, R. (1978). Radiation heat transfer. In *Augmented edition*. Washington, DC: Hemisphere Publ. Crop.

Waqas, M., Farooq, M., Khan, M. I., Alsaedi, A., Hayat, T., & Yasmeen, T. (2016). Magnetohydrodynamic (MHD) mixed convection flow of micropolar liquid due to nonlinear stretched sheet with convective condition. *International Journal of Heat and Mass Transfer*, *102*, 766–772.